Microscopic Theory of the Shape Memory Effect in TiNi

J. M. Zhang
Faculty of Mathematical Studies, University of Southampton, Southampton SO17 1BJ, United Kingdom

G. Y. Guo
Daresbury Laboratory, Warrington, Cheshire WA4 4AD, United Kingdom
(Received 19 August 1996)

An *ab initio* study of the Bain strain and orthorhombic distortions in the TiM compounds (M = Ni, Cu, Rh, Pd, and Ag) shows that the $B2$ structure of the shape memory alloy TiNi, unlike that of the other TiM compounds, is stable against these distortions, and that TiNi has some flat total energy minima. A thermodynamic model, built on these findings, displays some features of the shape memory effect. An electronic structure analysis reveals the importance of the Ni metallic bonding to the $B2$ phase stability and to the detwinning mechanism. [S0031-9007(97)03438-8]

PACS numbers: 62.20.Fe, 71.20.–b, 81.30.Kf

TiNi crystallizes in the cubic $B2$ (CsCl) structure at high temperatures. It undergoes a martensitic transformation (MT) to a low temperature monoclinic $\beta 19'$ structure (martensite) [1,2] at the MT temperature (M_s) of ~333 K [2]. The MT is accompanied by the shape memory effect (SME) [1,3]. The SME is an unusual mechanical deformation behavior. It arises when an alloy plastically deformed at some low temperature reverts to its original shape upon heating to some temperatures higher than A_s during the reverse transformation process. The A_s for TiNi is slightly (10–20 K) above the M_s. Experiments [3] have revealed that inside the martensite there are energetic equivalent domains separated by twinning boundaries which accommodate the reversible mechanical deformations through twinning processes. Furthermore, it has been concluded that a detwinning (or deshearing) mechanism is essential to the original shape backing process [3,4]. A tremendous amount of experimental and theoretical work on both MTs and SME (see, e.g., [1–7]) has been carried out because of their intrinsic fundamental interest and important technological applications. However, the theoretical understanding of the MTs is still incomplete, and no microscopic theory so far has been proposed to explain the SME.

In order to contribute to the atomic level understanding of the SME, we have carried out comparative total energy and electronic structure studies of the Bain transformation and orthorhombic distortions in five Ti-based intermetallic compounds TiM (M = Ni, Cu, Rh, Pd, and Ag). Interestingly, our total energy calculations show that the $B2$ structure of TiNi, unlike that of the other TiM compounds studied, is stable against these distortions, and there are energy barriers separating it from the martensite. This is perhaps why only TiNi, among these compounds, exhibits the SME. In this Letter, we describe a microscopic model case for the SME in TiNi and discuss the stability of the $B2$ structure and the SME in terms of the calculated electronic structures and free energies.

Self-consistent electronic band structure and total energy calculations of these compounds have been performed using the highly accurate full-potential linear augmented plane (FLAPW) method [8]. The calculations are based on the first-principles density function theory with the usual local density approximation (LDA) using the LDA exchange-correlation potential by Vosko *et al.* [9]. The special k-point Brillouin zone (BZ) integration method [10] was used, with 105 and 96 k points for the tetragonal and orthorhombic structures, respectively. The cutoff angular momentum, $L_{\max}$, is 12 for the wave functions and 6 for charge densities and potentials in the muffin-tin spheres. The number of the augmented plane waves included is about 100 to 125 per atom.

Bain strain [5,11] is a homogeneous tetragonal distortion measured by a single variable of the c/a ratio. It transforms, through a continuous change of c/a, the $B2$ structure ($c/a = 1$) to a fcc-based close-packed structure ($c/a = \sqrt{2}$). Here, we use the term $L1_0$ to refer to the intermediate, tetragonal phase with c/a other than 1. In Fig. 1 we plot the total energy for all the TiM compounds considered as a function of the Bain strain (c/a) with the volume fixed to the $B2$ minimum energy volume. We note that our theoretical results are consistent with experiments. For example, our results show that TiRh has a stable $L1_0$ with a c/a of 1.15, compared favorably with the experimental c/a value of 1.14 [2]. For TiCu the $L1_0$ structure with $c/a \approx 0.9$ [2] resulting from quenching is confirmed by our calculations. The theoretically indicated $L1_0$ with $c/a \approx 1.4$ may be prevented by the barrier at $c/a \approx 1.1$. TiAg [2] has a $L1_0$ with $c/a \approx 1.41$ being close to our theoretical result of $c/a \approx 1.5$. To identify particular features in the electronic structure of the TiM compounds which destabilize the $B2$ structure, we decompose the total energy (E_{tot}) in a traditional manner [12], as the sum of the one electron eigenvalue sum (or band energy) (E_{band}), the Madelung energy, and the so-called double counting term. We found that the Madelung

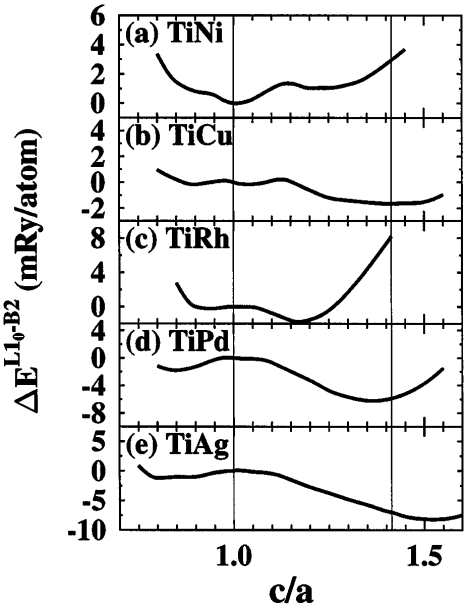

FIG. 1. Total energy $\Delta E_{\text{tot}}^{L1_0-B2}$ (relative to the $B2$ phase) of the TiM compounds as a function of c/a. The vertical lines at $c/a = 1$ and 1.41 denote, respectively, the $B2$ and fcc-based structures (see text).

energy [12] alone would stabilize the $B2$ against a Bain distortion in all the systems except TiRh where the Madelung energy is neutral for small Bain distortions. Thus, E_{band} seems to be the key factor controlling the instability of the $B2$ structure.

We found that the unusual feature of TiNi compared with the other TiM compounds is that the Ni-d orbitals are much less active than that of the other M transition metals. To illustrate this interesting bonding character, we show in Fig. 2 the differences between the valence charge densities and those obtained by a superposition of the atomic charge densities for TiNi and TiPd. Here Pd is taken as the representative of the other M transition metals. We note that in the c/a range from 1 to 1.05, the charge density around the Ni atoms is spherically symmetric and concentrated around the core region (i.e., metallic bonding). This may be further quantified by the ratio of the occupation number per d-t_{2g} state over the occupation number per d-e_g state. We found that the ratio for Ni is far closer to 1 than the other M atoms. In contrast, the d-t_{2g} orbitals of Pd are more extended and the bonding between Ti and Pd is directional even in the $B2$ structure (see Fig. 2). Interestingly, the Ni band energy tends to stabilize the $B2$ against the tetragonal shear (see Fig. 3) when the Ni is in the metallic bonding state. This behavior is not shared by any other M's band energy which, we found, is actually the major driving force of the transformation. Beyond $c/a = 1.05$, the directional bonding is built up between Ti and Ni as c/a further increases and, as a result, the Ni band energy is no longer to stabilize the $B2$ structure (see Fig. 3).

One could expect that the nondirectional Ni metallic bonding in the $B2$ TiNi would resist other structural deformations. Therefore, we further performed the FLAPW calculations for the orthorhombic distortions. The calculated total energy for TiNi is plotted against c/a and b/a_{B2} ($a_{B2} = a/\sqrt{2}$) in Fig. 4. Further details may be found in [13]. For TiNi, there is a metastable orthorhombic ($\beta 19$) phase [$a = 4.07$ Å, $b = 2.73$ Å, and $c = 4.64$ Å; Ni$(1/4, 0, \bar{z})$, $(3/4, 0, z)$, $z = 0.185$; Ti$(1/4, 1/2, z)$, $(3/4, 1/2, \bar{z})$, $z = 0.283$] which is about 1.4 mRy lower in total energy than the $B2$. Importantly, there is indeed an energy barrier of about 1.8 mRy/atom from the $\beta 19$ side between the two phases. Note that this $\beta 19$ phase is structurally and energetically close to the observed $\beta 19'$ ($a = 4.12$ Å, $b = 2.88$ Å, and $c = 4.62$ Å; Ni$(1/4, 0.027, \bar{z})$, $(3/4, 0.973, z)$, $z = 0.193$;

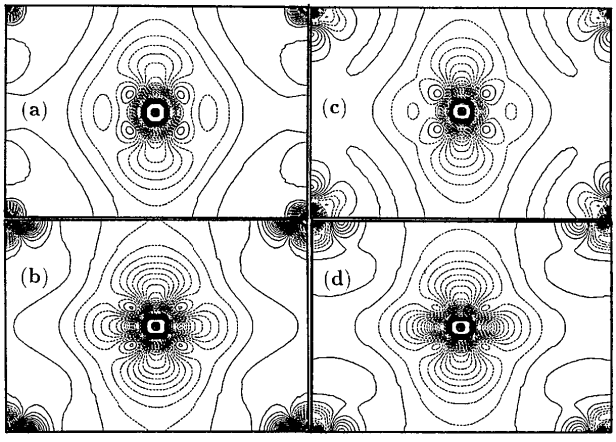

FIG. 2. Valence charge densities on the [110] plane (plotted as the differences between the valence charge densities and those obtained by a superposition of the free atomic charge densities) (in unit of $e/$ Å^3): (a) TiNi $c/a = 1$, (b) TiNi $c/a = 1.23$, (c) TiPd $c/a = 1$, and (d) TiPd $c/a = 1.23$. The increased and decreased charge densities are denoted with full lines and dashed lines, respectively.

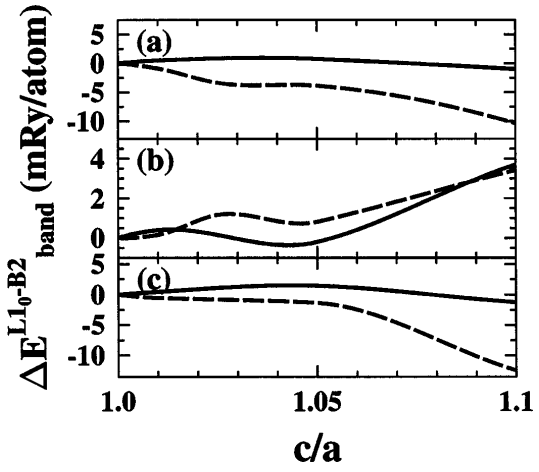

FIG. 3. Total and site-decomposed band energy differences between a $L1_0$ and the $B2$ structure, $\Delta E_{\text{band}}^{L1_0-B2}$, for TiNi (full lines) and TiPd (broken lines) as a function of c/a from 1 to 1.1: (a) $\Delta E_{\text{band-total}}^{L1_0-B2}$; (b) $\Delta E_{\text{band-Ti}}^{L1_0-B2}$; and (c) $\Delta E_{\text{band-Ni(Pd)}}^{L1_0-B2}$.

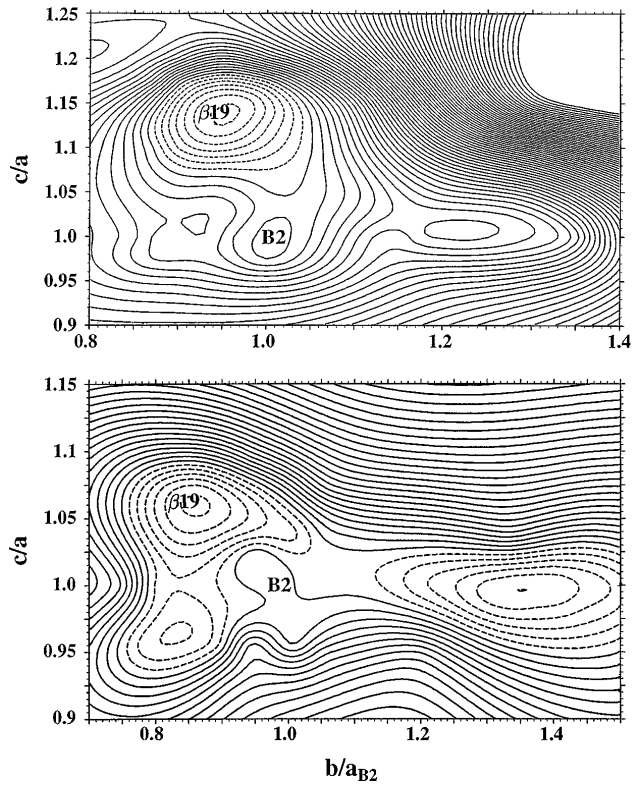

FIG. 4. Total energy of TiNi (upper) and TiPd (lower) as a function of c/a and b/a_{B2}. The energy difference between two adjacent contour lines is 0.2 mRy/atom for TiNi and 1.0 mRy/atom for TiPd. The dotted lines indicate the total energy being below that of the $B2$ phase.

Ti$(1/4, 0.553, z)$, $(3/4, 0.448, \bar{z})$, $z = 0.279$, $\gamma = 96.8°$ [14], and $\Delta E_{\text{tot}}^{B2-\beta 19'} \approx 1.7$ mRy/atom [15]). We also performed similar FLAPW total energy calculations for other TiM compounds and found that the $B2$ phases are always unstable against an orthorhombic distortion. We show in Fig. 4 the results for TiPd as a representative. The minimum total energy $\beta 19$ of TiPd has the structural parameters as $a = 4.58$ Å, $b = 2.75$ Å, and $c = 4.83$ Å; Pd$(1/4, 0, z)$, $(3/4, 0, \bar{z})$, $z = 0.697$; Ti$(1/4, 1/2, z)$, $(3/4, 1/2, \bar{z})$, $z = 0.197$, in good agreement with the observed $\beta 19$ [16].

The total energy for TiNi shown in Fig. 4 exhibits a rather flat local energy minimum at the $\beta 19$ phase. This means that when in the $\beta 19$ "martensite," TiNi would be rather insensitive to deformation, a characteristic shared by all shape memory alloys (SMA) [3,4]. We therefore construct a simple model case for the SME and in the following discussions take this metastable $\beta 19$ structure as the real martensite since the $\beta 19$ is close to the $\beta 19'$. Below, we calculate the free energy as a function of temperature along the minimum total energy path from the $B2$ to the $\beta 19$ martensite to see how a deformed specimen could recover its original shape when heated.

In the present free energy calculations, we included only the leading terms suggested by Watson and Weinert [17] and Moroni *et al.* [18]. Thus, the free energy difference is given as

$$\Delta G_{\text{tot}}(T) = \Delta E_{\text{tot}}(T) - T\Delta S_{\text{ele}}(T) + \Delta G_{\text{vib}}(T). \quad (1)$$

Here, the temperature dependence of $\Delta E_{\text{tot}}(T)$ is approximated by the energy change caused by the thermal excitation of the valence electrons $[\int EN(E) f dE - E_{\text{band}}(0)]$, where f is the Fermi distribution function and $N(E)$ the density of states. The electronic entropy $S_{\text{ele}}(T)$ is given by [17]

$$S_{\text{ele}}(T) = \int_0^T dT' \frac{1}{T'} \frac{d}{dT'} \int_{-\infty}^{+\infty} dE \frac{EN(E)}{e^{(E-\mu)/kT'} + 1}, \quad (2)$$

where μ is the chemical potential.

We obtained the vibrational free energy $G_{\text{vib}}(T)$ from the Debye temperature (Θ_D) using the general equation given in [19,20]. Anderson [20] showed that for an isotropic crystal the Θ_D can be derived from the averaged velocity $\bar{v}$ which, for cubic lattices, is related to the elastic constants B, C', and C_{44}. For a $\beta 19$ (orthorhombic) lattice, the sound velocity associated with shear and longitudinal modes is related to the various elastic constants (C_{ij}) in a complicated way [20]. Nevertheless, we noticed that for TiNi the $\beta 19$ and $\beta 19'$ structures are just a modified $B2$ structure with some minor variations. Thus, to make the Θ_D calculation for the $\beta 19$-TiNi tractable, we used the expressions for Θ_D for the cubic phase given by Anderson [20]. We also used the well established [6] elastic anisotropy value ($A = C_{44}/C'$) 0.6 for $\beta 19'$-TiNi and 2.0 for $B2$-TiNi to obtain the C_{44} for the $\beta 19$ and $B2$, respectively. For the other $\beta 19$ phases along the minimum energy path, the bulk modulus B and the shear constant C' are derived from our total energy calculations, but the A values are estimated through a linear interpolation between the values for the $B2$ and the $\beta 19$. Figure 5 shows that the calculated $S_{\text{vib}}(T)$ for the $B2$ and the $\beta 19$ phases are, respectively, in good agreement with the measured values for the $B2$ and the $\beta 19'$ phases. This

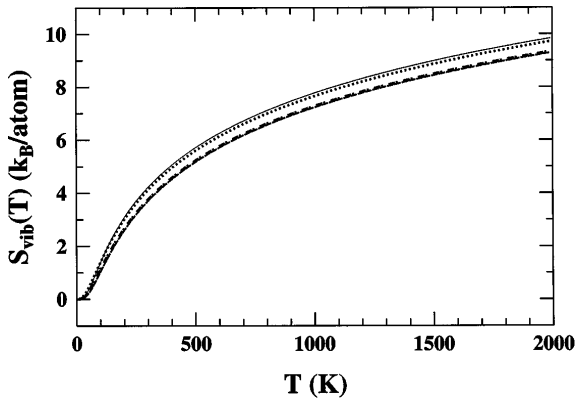

FIG. 5. The calculated TiNi $S_{\text{vib}}(T)$ (in unit of k_B/atom) for $B2$ (full line) and for $\beta 19$ (broken line) are compared with the $S_{\text{vib}}(T)$ for $B2$ (dotted line) and for $\beta 19'$ (chain line) derived from the measured phonon density of states [21].

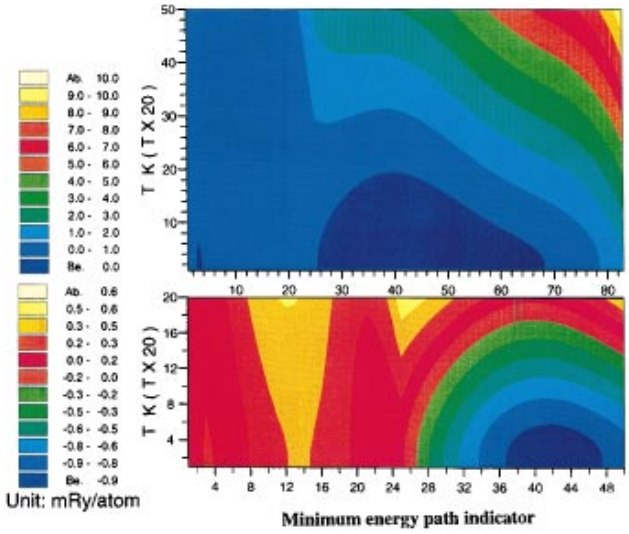

FIG. 6(color). TiNi free energy $\Delta G(T)$ (relative to the $B2$ phase) along the minimum energy path (see Fig. 4). The numbers on the horizontal axes merely indicate the distance from the $B2$ phase (at 0). The $\beta 19$ phase is at 42. The lower panel is an amplified image of the upper panel.

lends strong support to the principle underlying our $\Delta G(T)$ calculations. The calculated transformation temperature T_0 is 340 K, a value being nearly the same as the measured $T_0 \approx 340$ K between the $B2$ and the $\beta 19'$ phases. This is perhaps not surprising since, as noticed before, the $\beta 19$ phase is close to the $\beta 19'$ both geometrically and energetically.

The final results for the free energy $G(T)$ along the minimum energy path are shown in Fig. 6. Figure 6 shows some SME behaviors as follows: At low temperatures a specimen in the martensitic state would be ductile and easily extended or compressed. When heated to sufficient high temperatures, it reverts to the original $B2$ phase because the martensite is now unstable and its shape is recovered since the deformation can no longer be sustained in the $B2$ structure.

In conclusion, from the electronic structure viewpoint, the specimen which grows to remember the undeformed condition may be regarded as a direct result of the shift from the covalent bonding in the martensite to the metallic one in the $B2$. Therefore, the unique Ni metallic bonding in the $B2$ structure which appears to be the principal source of the $B2$ stability, is also the main driving force in the detwinning process.

J. M. Z. thanks Professor T. Sluckin and Professor P. T. Landsberg for their support and encouragement in the past years.

[1] F. E. Wang, W. Y. Buchler, and S. Y. Pickart, J. Appl. Phys. **36**, 3232 (1965).
[2] P. Rogl, in *Atomic Energy Review, Special Issue 9*, edited by K. L. Komarek (International Atomic Energy Agency, Vienna, 1983).
[3] C. M. Wayman, Mater. Res. Soc. Symp. Proc. **21**, 657 (1984).
[4] K. Otsuka, Jpn. J. Appl. Phys. **10**, 571 (1971).
[5] Z. Nishiyama, *Martensitic Transformations* (Academic, New York, 1978).
[6] T. M. Brill *et al.*, J. Phys. Condens. Matter **3**, 9621 (1991).
[7] G. L. Zhao, T. C. Leung, and B. N. Harmon, Phys. Rev. B **40**, 7999 (1989).
[8] P. Blaha *et al.*, Comput. Phys. Commun. **59**, 399 (1990).
[9] S. H. Vosko, L. Wilk, and M. Nusair, Can. J. Phys. **58**, 1200 (1980).
[10] H. J. Monkhorst and J. D. Pack, Phys. Rev. B **13**, 5188 (1976).
[11] P. E. A. Turchi, Mater. Sci. Eng. A **127**, 145 (1990).
[12] M. Weinert, E. Wimmer, and A. J. Freeman, Phys. Rev. B **26**, 4571 (1982).
[13] J. M. Zhang, Ph.D. thesis, Southampton University, 1997.
[14] G. M. Michal and R. Sinclair, Acta Crystallogr. **37**, 1804 (1981).
[15] D. N. AbuJudom, P. E. Thoma, and S. Fariabi, Mater. Sci. Forum **56-58**, 565 (1990).
[16] G. Bihlmayer, R. Eibler, and A. Neckel, J. Phys. Condens. Matter **5**, 5083 (1993).
[17] R. E. Watson and M. Weinert, Phys. Rev. B **30**, 1641 (1984).
[18] E. G. Moroni, G. Grimvall, and T. Jarlborg, Phys. Rev. Lett. **76**, 2758 (1996).
[19] V. L. Moruzzi, J. F. Janak, and K. Schwarz, Phys. Rev. B **37**, 790 (1988).
[20] O. L. Anderson, in *Physical Acoustics*, edited by W. P. Mason (Academic, New York, 1965), Vol. III-B.
[21] G. Herget *et al.*, Europhys. Lett. **10**, 49 (1989).